Regularized Nonrigid Registration of Lung CT Images by Preserving Tissue Volume and Vesselness Measure

Kunlin Cao[1,3], Kaifang Du[2,3], Kai Ding[2,3], Joseph M. Reinhardt[2,3,*], and Gary E. Christensen[1,3]

[1] Department of Electrical and Computer Engineering
[2] Department of Biomedical Engineering
[3] The Iowa Institute for Biomedical Imaging and
The Iowa Comprehensive Lung Imaging Center
The University of Iowa, Iowa City, 52242

Abstract. Image registration is an important research area within pulmonary image analysis. Accurate registration is critical to post-analysis of lung mechanical properties and useful for clinical applications. To improve registration accuracy, we design a nonrigid registration algorithm to preserve both parenchymal tissue volume and vesselness measure. In addition, the transformation is regularized using a Laplacian constraint. Comparison experiments are performed and evaluation statistics demonstrate this algorithm has achieved better registration accuracy in the alignment of lung boundaries, fissures, and landmarks. Visual inspection shows obvious improvement on matching accuracy in the lung regions near the thoracic cage. This algorithm also results in physiologically more plausible Jacobian patterns.

1 Introduction

The respiratory system's function is to provide gas exchange. Understanding the ventilation patterns of lung parenchyma is important for many clinical applications such as disease detecting and therapy planning [1]. Imaging allows non-invasive study of lung behaviors, and image registration can be used to match images acquired at different inflation levels to examine the mechanical properties of lung parenchyma. Therefore, accurate registration techniques of thoracic CT images is useful in practice and also challenging due to the elastic nature of lung deformation. Christensen et al. [2] used the sum of squared intensity difference (SSD) consistent linear elastic image registration to match images across cine-CT sequences, and estimate rates of local tissue expansion and contraction. Yin et al. [3] proposed a new similarity cost function preserving the lung tissue volume and compared the new cost function driven registration with SSD driven registration in the estimation of regional lung function. Cao et

* Joseph M. Reinhardt is a shareholder in VIDA Diagnostics, Inc.

al. [4] utilized the rich information of vessel locations and shapes, and introduced a similarity criterion to help match the vessel structures.

In this paper, we design a registration algorithm which combines the similarity criteria of preserving tissue volume and vesselness measure together, and uses a Laplacian constraint to regularize the transformation. This algorithm is used to register data sets from 20 different subjects. Comparison experiments demonstrates its ability to accurately catch lung deformations during respiration on various kinds of data.

2 Methods

2.1 Data Acquisition

Twenty pairs of volumetric chest CT scans are used in the study. Each pair of scans is taken from a single subject, which may exhibit lung disease or appear healthy. Data are acquired from a variety of scanners and thus contain a variety of image resolutions. The parenchyma regions for each scan are identified as lung region masks. Full details of data acquisition for each subject are described in [5].

2.2 Image Registration and Transformation Parameterization

Image registration is used to find an optimal spatial transform that maps points from the moving image I_{mov} to the corresponding points in the fixed image I_{fix}. Let $\mathbf{x} = [x_1, x_2, x_3]^T$ define a voxel coordinate in the image domain. Transformation $\mathbf{h}$ is a 3×1 vector-valued function defined on the voxel lattice. At location $\mathbf{x}$ in the fixed image, $\mathbf{h}(\mathbf{x})$ gives its corresponding location in the moving image.

The B-Spline based parameterization is chosen to represent the transformation. Let $\phi_i = [\phi_x(\mathbf{x}_i), \phi_y(\mathbf{x}_i), \phi_z(\mathbf{x}_i)]^T$ be the coefficients of the i-th control point $\mathbf{x}_i$ on the spline lattice G along each direction. The transformation is represented as

$$\mathbf{h}(\mathbf{x}) = \mathbf{x} + \sum_{i \in G} \phi_i \beta^{(3)}(\mathbf{x} - \mathbf{x}_i), \tag{1}$$

where $\beta^{(3)}(\mathbf{x}) = \beta^{(3)}(x)\beta^{(3)}(y)\beta^{(3)}(z)$ is a separable convolution kernel. $\beta^{(3)}(x)$ is the uniform cubic B-Spline basis function.

2.3 Intensity-based Matching Criterion

The intensity matching criterion is used to register similar grayscale patterns in two images. CT intensity is a measure of tissue density and therefore changes as the tissue density changes during inflation and deflation. To take the variation of intensity during respiration into account, the sum of squared tissue volume difference (SSTVD) [3] is used as the intensity similarity criterion to preserve tissue volume. This similarity criterion aims to minimize the local difference of tissue volume inside the lungs scanned at different pressure levels. Assume the Hounsfield units (HU) of CT lung images are primarily contributed by tissue

and air. Then, the tissue volume in a voxel at position $\mathbf{x}$ can be estimated as $V(\mathbf{x}) = v(\mathbf{x})\frac{HU(\mathbf{x})-HU_{air}}{HU_{tissue}-HU_{air}}$ where $v(\mathbf{x})$ is the volume of voxel $\mathbf{x}$. It is assumed that $HU_{air} = -1000$ and $HU_{tissue} = 55$. The intensity similarity metric SSTVD is defined as [3]

$$C_{\text{SSTVD}} = \int_{\mathbf{\Omega}} \left[V_{fix}(\mathbf{x}) - V_{mov}(\mathbf{h}(\mathbf{x}))\right]^2 d\mathbf{x} \tag{2}$$
$$= \int_{\mathbf{\Omega}} \left[v_{fix}(\mathbf{x})\frac{I_{fix}(\mathbf{x})+1000}{1055} - v_{mov}(\mathbf{h}(\mathbf{x}))\frac{I_{mov}(\mathbf{h}(\mathbf{x}))+1000}{1055}\right]^2 d\mathbf{x}$$

where Ω denotes the lung region of the target image. The Jacobian of a transformation $J(\mathbf{h})$ estimates the local volume changes resulted from mapping an image through the deformation. Thus, the tissue volume in image I_{mov} and I_{fix} are related by $v_{mov}(\mathbf{h}(\mathbf{x})) = v_{fix}(\mathbf{x}) \cdot J(\mathbf{h}(\mathbf{x}))$.

2.4 Feature-based Matching Criterion (SSVMD)

Blood vessels have larger HU than that of parenchymal tissues. This intensity contrast is low at small vessels and thus gives almost no contribution to intensity-based similarity metric. In order to better utilize the information of vessel locations, we use the vesselness measure (VM) extracted from intensity image.

The vesselness measure is based on the analysis of eigenvalues of the Hessian matrix of image intensity. The eigenvalues, ordered by magnitude $|\lambda_1| \leq |\lambda_2| \leq |\lambda_3|$, are geometrically interpreted as principal curvatures and can be used to indicate the shape of underlying object. In 3D lung CT images, isotropic structures such as parenchyma tissues are associated with three similar non-zero positive eigenvalues while tubular structures such as blood vessels are associated with one negligible eigenvalue and two similar non-zero negative eigenvalues [6]. The vesselness measure is computed from the Frangi's vesselness function [6]

$$F(\lambda) = \begin{cases} (1 - e^{-\frac{R_A^2}{2\alpha^2}}) \cdot e^{\frac{-R_B^2}{2\beta^2}} \cdot (1 - e^{-\frac{S^2}{2\gamma^2}}) \; if \; \lambda_2 < 0 \; and \; \lambda_3 < 0 \\ 0 \qquad\qquad\qquad\qquad\qquad\qquad otherwise \end{cases} \tag{3}$$

with $R_A = \frac{|\lambda_2|}{|\lambda_3|}, R_B = \frac{|\lambda_1|}{\sqrt{|\lambda_2\lambda_3|}}, S = \sqrt{\lambda_1^2 + \lambda_2^2 + \lambda_3^2}$. α, β, γ control the sensitivity of the vesselness measure. The experiments in this paper use $\alpha = 0.5$, $\beta = 0.5$, and $\gamma = 5$.

The vesselness image is rescaled to $[0, 1]$ and can be considered as a probability-like estimate of vesselness features. Larger vesselness value indicates the underlying object is more likely to be a vessel structure. As shown in Figure 1, the vesselness measurement enhances blood vessel information. The sum of squared vesselness measure difference (SSVMD) is designed to match similar vesselness patterns in two images. Given F_{mov} and F_{fix} as the vesselness measures of images I_{mov} and I_{fix}, respectively, this cost function is formed as

$$C_{\text{SSVMD}} = \int_{\mathbf{\Omega}} \left[F_{fix}(\mathbf{x}) - F_{mov}(\mathbf{h}(\mathbf{x}))\right]^2 d\mathbf{x}. \tag{4}$$

Mismatch from vessel to tissue structures will result in a larger SSVMD cost.

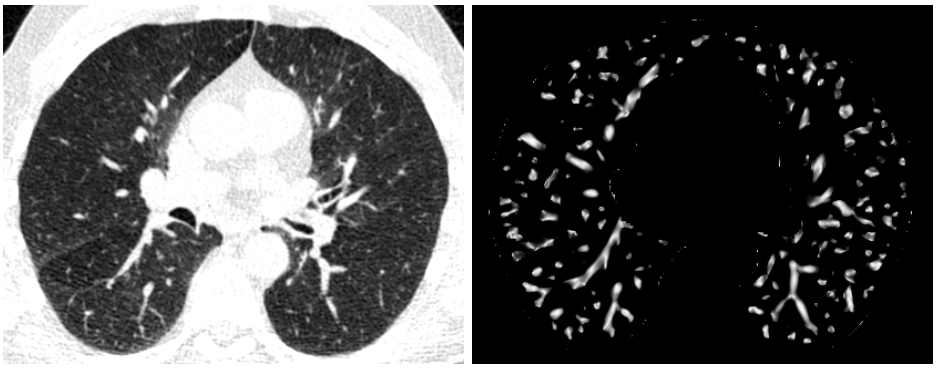

(a) (b)

Fig. 1. The vesselness images calculated from lung CT grayscale images. (a) A transverse slice of FRC data. (b) The vesselness measure of slice in (a).

2.5 Laplacian Regularization Constraint (LAP)

Enforcing constraints on the transformation helps generate physiologically more meaningful registration results. Continuum mechanical models such as linear elasticity can be used to regularize the transformations. In this paper, a Laplacian operator is used to regularize the displacement fields $\mathbf{u}$ where $\mathbf{u} = \mathbf{h}(\mathbf{x}) - \mathbf{x}$. This regularization term is formed as

$$C_{\mathrm{LAP}} = \int_{\mathbf{\Omega}} ||\nabla^2 \mathbf{u}(\mathbf{x})||^2 d\mathbf{x}. \tag{5}$$

where $\nabla = \left[\frac{\partial}{\partial x_1}, \frac{\partial}{\partial x_2}, \frac{\partial}{\partial x_3}\right]$ and $\nabla^2 = \nabla \cdot \nabla = \left[\frac{\partial^2}{\partial x_1^2} + \frac{\partial^2}{\partial x_2^2} + \frac{\partial^2}{\partial x_3^2}\right]$. Using linear elasticity differential operator can help smooth the transformation, and help eliminate abrupt changes in the displacement fields.

2.6 Multi-Resolution Scheme and Estimation

A spatial multiresolution procedure from coarse to fine is used in the registration in order to improve speed, accuracy and robustness. The multiresolution strategy used in the experiments proceeds from low to high resolution starting at one-fourth the spatial resolution and increases by a factor of two until the full resolution is reached. Meanwhile, a hierarchy of B-Spline grid spacings from large to small is used. The multiresolution scheme for minimizing the total cost function is listed in Table 1. The images and grid spacing are refined alternatively.

For each pair of lung CT images, registrations using three cost functions are performed for comparison. They are three algorithms driven by: (1) C_{SSTVD}, (2) $C_{\mathrm{SSTVD}} + \rho_1 C_{\mathrm{SSVMD}}$, (3) $C_{\mathrm{SSTVD}} + \rho_1 C_{\mathrm{SSVMD}} + \rho_2 C_{\mathrm{LAP}}$. For convenience, we will name them Alg. 1, Alg. 2 and Alg. 3, respectively. The experiments in this paper use $\rho_1 = 0.75$, and $\rho_2 = 0.01$.

Image resolution	B-Spline grid size	Max. Iteration
1/4	128 mm $\longrightarrow$ 64 mm $\longrightarrow$ 32 mm $\longrightarrow$ 16 mm	4000
1/2	16 mm $\longrightarrow$ 8 mm	400
1	8 mm $\longrightarrow$ 4 mm	40

Table 1. Multi-Resolution Scheme

The similarity cost functions are optimized using a limited-memory, quasi-Newton minimization method with bounds (L-BFGS-B) [7] algorithm which is well suited for optimization with a high dimensional parameter space. This algorithm allows bound constraints on the independent variables. Choi and Lee [8] have proposed the sufficient conditions to guarantee the local injectivity (one-to-one property) of functions parameterized by uniform cubic B-Spline, which is used here in the optimization to constrain the B-Spline coefficients so that the transformation maintains the topology of two images. According to their analysis, the displacement fields are locally injective all over the domain if B-Spline coefficients satisfy the condition that $\phi_x \leq \delta_x/K, \phi_y \leq \delta_y/K, \phi_z \leq \delta_z/K$, where $\delta_x, \delta_y, \delta_z$ are the B-Spline grid sizes along each direction, and K is a constant approximately equal to 2.479772335.

3 Experiments and Results

Processing starts by resampling the input fixed and moving images to a voxel size of 1 mm $\times$ 1 mm $\times$ 1 mm. After resampling, an affine registration is first applied to initialize the matching process from the moving image I_{mov} to the fixed image I_{fix}. It is implemented within ITK's registration framework using mutual information similarity measure, linear interpolation, and regular step gradient descent optimizer. No masks are used in the affine registration. Then the B-Spline based registration algorithm described in Section 2 is applied on the lung parenchyma regions. After the registration is done, the displacement fields are then resampled to the original voxel size as that of I_{fix}. All three algorithms are fully automatic, and the parameters are fixed for all registration pairs. For each registration, the three algorithms use the same common parameter settings.

All the registration results are evaluated in the following four separate aspects: (1) alignment of the lung boundaries, (2) alignment of the major fissures, (3) alignment of correspondence of annotated point pairs, (4) analysis of singularities in the deformation field. Full details of the evaluation methods can be found in [5]. The results for Alg. 1, Alg. 2, and Alg. 3 are listed in Table 2, Table 3, and Table 4, respectively. In general, a lower score is better than a higher score, and is associated with a higher rank.

For comparison of the three registration algorithms, the rank statistics are plotted in Figure 2 (a) through all 20 subjects. Figure 2 (b) shows the box-plot of rank statistics resulted from three algorithms. Alg. 3 performs best according to the four evaluation aspects.

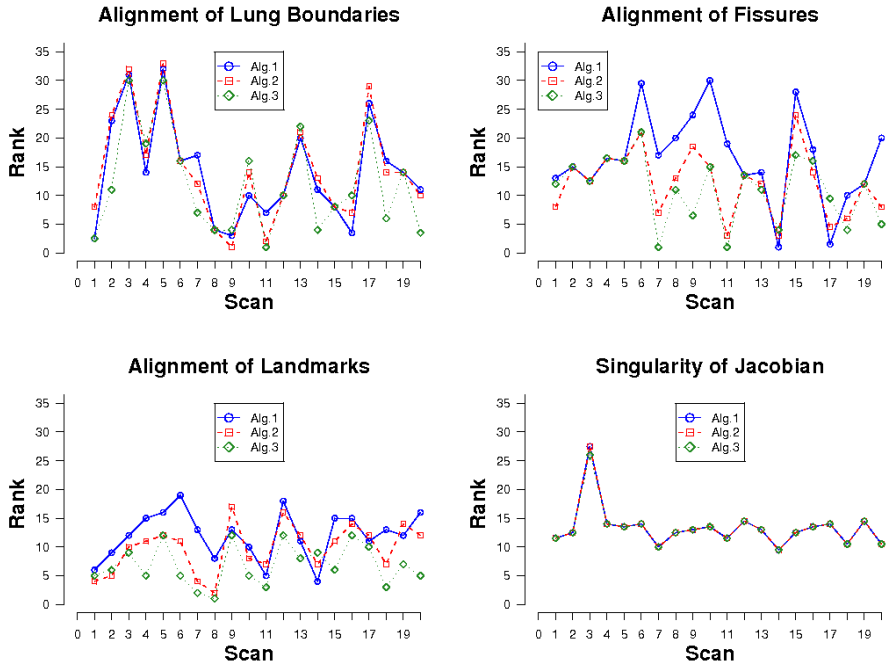

(a)

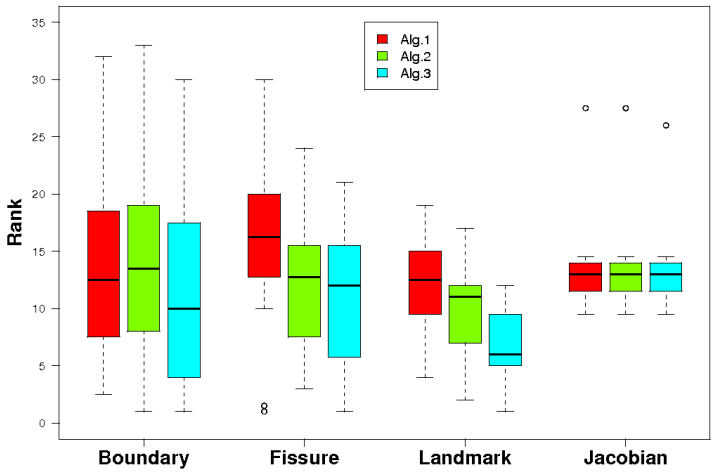

(b)

Fig. 2. (a) Rank statistics resulted from three registration methods on alignment of lung boundaries, fissures, landmarks, and singularity of Jacobian; (b) Box-plot of rank statistics resulted from three algorithms through four evaluation aspects.

An example of registration results on a sagittal slice is illustrated in Figure 3. The fused images of a fixed slice (colored red) and its deformed slice (colored green), and their corresponding Jacobian maps resulted from three registration algorithms are shown for comparison. Large matching errors are reduced after adding the SSVMD constraint. Laplacian term helps regularize the transformation, and further increase the matching accuracy. In order to reveal the lung tissue deformation pattern, the Jacobian was used to estimate the local tissue deformation (and thus, specific volume change) of the transformation field derived by image registration [9, 10]. Using a Lagrangian reference frame, local tissue expansion corresponds to a Jacobian greater than one and local tissue contraction corresponds to a Jacobian less than one.

	Lung Boundaries		**Fissures**		**Landmarks**		**Singularities**	
Scan Pair	**Score**	**Rank**	**Score**	**Rank**	**Score**	**Rank**	**Score**	**Rank**
01	0.00	2.50	0.18	13.00	1.64	6.00	0.00	11.50
02	0.00	23.00	0.00	15.00	0.38	9.00	0.00	12.50
03	0.02	31.00	0.00	12.50	0.37	12.00	0.00	27.50
04	0.00	14.00	0.00	16.50	1.28	15.00	0.00	14.00
05	0.11	32.00	0.00	16.00	0.02	16.00	0.00	13.50
06	0.00	16.00	0.00	29.50	0.40	19.00	0.00	14.00
07	0.03	17.00	1.23	17.00	2.59	13.00	0.00	10.00
08	0.00	4.00	0.31	20.00	0.76	8.00	0.00	12.50
09	0.00	3.00	0.00	24.00	0.57	13.00	0.00	13.00
10	0.00	10.00	0.00	30.00	1.52	10.00	0.00	13.50
11	0.00	7.00	0.17	19.00	0.66	5.00	0.00	11.50
12	0.00	10.00	0.00	13.50	0.08	18.00	0.00	14.50
13	0.00	20.00	0.09	14.00	0.86	11.00	0.00	13.00
14	0.01	11.00	0.15	1.00	1.60	4.00	0.00	9.50
15	0.00	8.00	0.00	28.00	0.67	15.00	0.00	12.50
16	0.00	3.50	0.08	18.00	1.14	15.00	0.00	13.50
17	0.00	26.00	0.02	1.50	0.83	11.00	0.00	14.00
18	0.04	16.00	0.96	10.00	2.76	13.00	0.00	10.50
19	0.00	14.00	0.00	12.00	0.49	12.00	0.00	14.50
20	0.00	11.00	4.40	20.00	2.80	16.00	0.00	10.50
Avg	0.01	13.95	0.38	16.52	1.07	12.05	0.00	13.30
Average Ranking Overall								13.95
Final Placement								10

Table 2. Alg. 1 results for each scan pair, per category and overall. Rankings and final placement are from a total of 34 competing algorithms.

4 Discussion

Tables 2 - 4 and Figure 2 show that adding the SSVMD cost function and the Laplacian regularization term helps improve the registration accuracy comparing with using basic SSTVD similarity cost alone. Alg. 2 utilizes enhanced vesselness information and uses SSVMD to help match the vessels. Compared with Alg. 1, Alg. 2 achieves higher ranks on fissure and landmark alignment, but not on boundary alignment. This demonstrates that SSVMD can help match structures within the lung more accurately. Alg. 3 has a Laplacian term combined to regularize the displacement fields to be elastic, which makes the transformation more mechanically meaningful. Among the three algorithms, Alg. 3 achieves the best rank on alignment of lung boundaries, fissures, and landmarks. All three

	Lung Boundaries		**Fissures**		**Landmarks**		**Singularities**	
Scan Pair	**Score**	**Rank**	**Score**	**Rank**	**Score**	**Rank**	**Score**	**Rank**
01	0.00	8.00	0.03	8.00	1.23	4.00	0.00	11.50
02	0.00	24.00	0.00	15.00	0.35	5.00	0.00	12.50
03	0.02	32.00	0.00	12.50	0.36	10.00	0.00	27.50
04	0.00	17.00	0.00	16.50	1.10	11.00	0.00	14.00
05	0.12	33.00	0.00	16.00	0.01	12.00	0.00	13.50
06	0.00	16.00	0.00	21.00	0.34	11.00	0.00	14.00
07	0.00	12.00	0.48	7.00	1.43	4.00	0.00	10.00
08	0.00	4.00	0.01	13.00	0.57	2.00	0.00	12.50
09	0.00	1.00	0.00	18.50	0.61	17.00	0.00	13.00
10	0.00	14.00	0.00	15.00	1.18	8.00	0.00	13.50
11	0.00	2.00	0.00	3.00	0.69	7.00	0.00	11.50
12	0.00	10.00	0.00	13.50	0.07	16.00	0.00	14.50
13	0.00	21.00	0.08	12.00	0.90	12.00	0.00	13.00
14	0.02	13.00	0.28	3.00	1.89	7.00	0.00	9.50
15	0.00	8.00	0.00	24.00	0.64	11.00	0.00	12.50
16	0.00	7.00	0.05	14.00	1.08	14.00	0.00	13.50
17	0.00	29.00	0.03	4.50	0.83	12.00	0.00	14.00
18	0.01	14.00	0.17	6.00	1.84	7.00	0.00	10.50
19	0.00	14.00	0.00	12.00	0.50	14.00	0.00	14.50
20	0.00	10.00	1.82	8.00	1.90	12.00	0.00	10.50
Avg	0.01	14.45	0.15	12.12	0.88	9.80	0.00	13.30
Average Ranking Overall								12.41
Final Placement								5

Table 3. Alg. 2 results for each scan pair, per category and overall. Rankings and final placement are from a total of 34 competing algorithms.

algorithms perform almost the same on evaluation of Jacobian singularity. This is because the B-Spline coefficients are bounded to ensure the injectivity of the transformation in their optimization process.

Figure 3 shows a case where the parenchyma regions are difficult to register due to the large discrepancies between low dose image acquired during inspiration (moving image) and ultra-low dose image acquired during expiration (fixed image). The parenchyma around lung boundaries are unsatisfactorily aligned using basic SSTVD metric alone, shown as the scattered red and green colors in the arrow pointing regions in Figure 3 (a). Their associated Jacobian patterns are also distorted. Those mismatches are much better aligned when SSVMD is used, as shown in Figure 3 (c). The reason for this is that blood vessels in those regions near lung boundaries are usually small and have low intensity con-

	Lung Boundaries		**Fissures**		**Landmarks**		**Singularities**	
Scan Pair	**Score**	**Rank**	**Score**	**Rank**	**Score**	**Rank**	**Score**	**Rank**
01	0.00	2.50	0.05	12.00	1.37	5.00	0.00	11.50
02	0.00	11.00	0.00	15.00	0.36	6.00	0.00	12.50
03	0.01	30.00	0.00	12.50	0.35	9.00	0.00	26.00
04	0.00	19.00	0.00	16.50	0.90	5.00	0.00	14.00
05	0.09	30.00	0.00	16.00	0.01	12.00	0.00	13.50
06	0.00	16.00	0.00	21.00	0.29	5.00	0.00	14.00
07	0.00	7.00	0.04	1.00	1.19	2.00	0.00	10.00
08	0.00	4.00	0.00	11.00	0.43	1.00	0.00	12.50
09	0.00	4.00	0.00	6.50	0.56	12.00	0.00	13.00
10	0.00	16.00	0.00	15.00	1.01	5.00	0.00	13.50
11	0.00	1.00	0.00	1.00	0.64	3.00	0.00	11.50
12	0.00	10.00	0.00	13.50	0.05	12.00	0.00	14.50
13	0.00	22.00	0.08	11.00	0.82	8.00	0.00	13.00
14	0.00	4.00	0.48	4.00	2.14	9.00	0.00	9.50
15	0.00	8.00	0.00	17.00	0.63	6.00	0.00	12.50
16	0.00	10.00	0.07	16.00	1.03	12.00	0.00	13.50
17	0.00	23.00	0.04	9.50	0.78	10.00	0.00	14.00
18	0.00	6.00	0.08	4.00	1.44	3.00	0.00	10.50
19	0.00	14.00	0.00	12.00	0.46	7.00	0.00	14.50
20	0.00	3.50	0.79	5.00	1.34	5.00	0.00	10.50
Avg	0.00	12.05	0.08	10.97	0.79	6.85	0.00	13.22
Average Ranking Overall								10.77
Final Placement								3

Table 4. Alg. 3 results for each scan pair, per category and overall. Rankings and final placement are from a total of 34 competing algorithms.

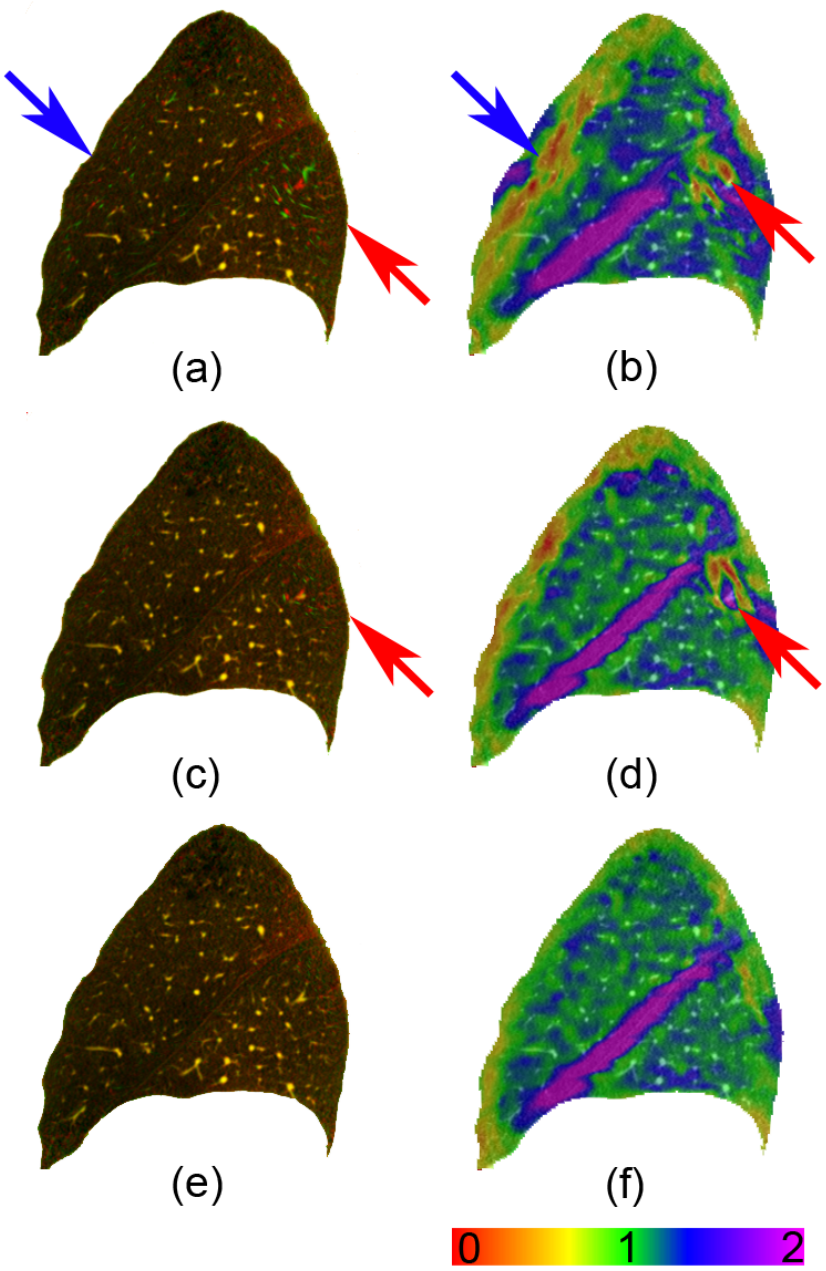

Fig. 3. The fused images of a fixed slice (colored red) and its deformed slice (colored green) resulted from three registration methods: (a) Alg. 1, (c) Alg. 2, and (e) Alg. 3. And their corresponding Jacobian maps are shown in (b), (d), and (f), respectively. Arrows denote regions of large discrepancies between the fixed and deformed slice. Note that the errors in these regions are reduced after adding the SSVMD and Laplacian constraint to the registration algorithm.

trast, and thus contribute little to conventional intensity similarity criterion. The vesselness measurement enhances blood vessel information and strengthens contribution of small vessels near the thoracic cage. Using SSVMD also helps correct the distortion of Jacobian patterns in some extent. However, matching errors and distortion in the Jacobian map still exist in the region pointed by red arrow. Combined with Laplacian constraint, Alg. 3 has the least matching errors in the result shown in Figure 3 (e). Since its displacements are regularized during optimization, the resulting transformation is much smoother, which results in less sudden changes and thus less distortions. Figure 3 (f) also suggests that the parenchymal tissues near the fissure have larger deformations, and the vessel structures have less volume changes comparing with parenchymal tissues during respiration.

5 Conclusion

We have described a regularized registration algorithm by preserving both tissue volume and vesselness measure. To evaluate the usage of the constraints SSVMD and LAP, experiments are performed to register the same groups of data using registration algorithms driven by SSTVD, SSTVD + SSVMD, and SSTVD + SSVMD + LAP. Results are presented to show that adding SSVMD and LAP constraints effectively improves the registration accuracy and provides a more reliable pattern of local lung tissue deformation. The purpose of adding SSVMD and LAP in the registration process is that it can help correct the mismatches of small vessels and their surrounding lung tissues. In this paper, the Laplacian operator is used to regularize the displacements to illustrate the importance and effectiveness of regularizing the transformations during registration process. More complicated continuum mechanical models [11, 12] can be used to regularize the transformations and will be tested in the future.

6 Acknowledgments

This work was supported by the NIH grants HL079406, HL64368, EB004126, HL080285, and CA129022.

References

1. Ding, K., Bayouth, J.E., Buatti, J.M., Christensen, G.E., Reinhardt, J.M.: 4DCT-based measurement of changes in pulmonary function following a course of radiation therapy. Medical Physics **37**(3) (2010) 1261–1272
2. Christensen, G.E., Song, J.H., Lu, W., Naqa, I.E., Low, D.A.: Tracking lung tissue motion and expansion/compression with inverse consistent image registration and spirometry. Medical Physics **34**(6) (2007) 2155–2165
3. Yin, Y., Hoffman, E.A., Lin, C.L.: Mass preserving non-rigid registration of CT lung images using cubic B-spline. Medical Physics **36**(9) (2009) 4213–4222

4. Cao, K., Ding, K., Christensen, G.E., Raghavan, M.L., Amelon, R.E., Reinhardt, J.M.: Unifying vascular information in intensity-based nonrigid lung ct registration. In: 4th International Workshop on Biomedical Image Registration. LCNS 6204, Springer (2010) 1–12
5. Murphy, K., van Ginneken, B., Reinhardt, J., Kabus, S., Ding, K., Deng, X., Pluim, J.: Evaluation of methods for pulmonary image registration: The EMPIRE10 study. In: Grand Challenges in Medical Image Analysis. (2010)
6. Frangi, A.F., Niessen, W.J., Vincken, K.L., Viergever, M.A.: Multiscale vessel enhancement filtering. In: MICCAI. Volume 1496. (1998) 130–137
7. Byrd, R.H., Lu, P., Nocedal, J., Zhu, C.: A limited memory algorithm for bound constrained optimization. SIAM J. Sci. Comput. **16**(5) (1995) 1190–1208
8. Choi, Y., Lee, S.: Injectivity conditions of 2d and 3d uniform cubic b-spline functions. Graphical Models **62**(6) (2000) 411–427
9. Reinhardt, J.M., Ding, K., Cao, K., Christensen, G.E., Hoffman, E.A., Bodas, S.V.: Registration-based estimates of local lung tissue expansion compared to xenon-CT measures of specific ventilation. Medical Image Analysis **12**(6) (2008) 752–763
10. Ding, K., Cao, K., Christensen, G.E., Hoffman, E.A., Reinhardt, J.M.: Registration-based regional lung mechanical analysis: Retrospectively reconstructed dynamic imaging versus static breath-hold image acquisition. In: Proc. SPIE Conf. Medical Imaging. Volume 7262. (2009) 72620D
11. Christensen, G.E., Joshi, S.C., Miller, M.I.: Volumetric transformation of brain anatomy. IEEE Trans. on Med. Imaging **16**(6) (1997) 864–877
12. Christensen, G.E., Rabbitt, R.D., Miller, M.I.: Deformable templates using large deformation kinematics. IEEE Trans. Image Proc. **5**(10) (1996) 1435–1447